Dalton Transactions

Accepted Manuscript

ROYAL SOCIETY OF CHEMISTRY

www.rsc.org/dalton

Based on energy transfer from Ce^{3+} to Eu^{2+}, a novel White-Light-Emitting $Ca_4(PO_4)_2O:Ce^{3+},Eu^{2+}$ phosphor was obtained.

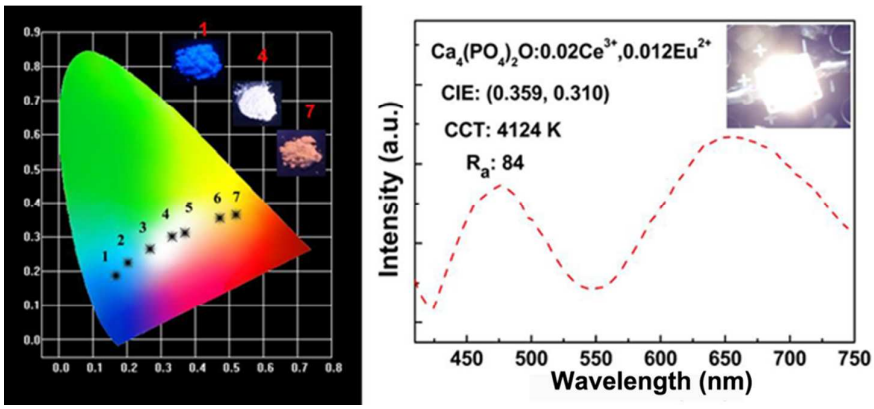

Journal Name

RSCPublishing

ARTICLE

Single-Phased White-Light-Emitting $Ca_4(PO_4)_2O:Ce^{3+},Eu^{2+}$ Phosphors Based on Energy Transfer

Cite this: DOI: 10.1039/x0xx00000x

Received 00th January 2012,
Accepted 00th January 2012

DOI: 10.1039/x0xx00000x

www.rsc.org/

Yonglei Jia,[ab] Ran Pang,[a] Haifeng Li,[ab] Wenzhi Sun,[ab] Jipeng Fu,[ab] Lihong Jiang,[a] Su Zhang,[a] Qiang Su,[a] Chengyu Li*[a] and Ru-Shi Liu*[cd]

A novel single-composition $Ca_4(PO_4)_2O:Ce^{3+},Eu^{2+}$ phosphor emitting white light was synthesized by conventional solid-state reactions for light-emitting diode applications. X-ray diffraction, photoluminescence spectra, and luminescence decay spectra were used to characterize the samples. Energy transfer from Ce^{3+} to Eu^{2+} ions was observed in the co-doped samples, and the transfer mechanism in the $Ca_4(PO_4)_2O:Ce^{3+},Eu^{2+}$ phosphors was dipole–dipole interaction. The emission hue of $Ca_4(PO_4)_2O:Ce^{3+},Eu^{2+}$ was found to vary from blue (0.165, 0.188) to white (0.332, 0.300) and eventually to orange (0.519, 0.366) by precisely controlling the ratio of Ce^{3+} to Eu^{2+}. The combination of a 380-nm near-ultraviolet chip with $Ca_4(PO_4)_2O:0.02Ce^{3+},0.012Eu^{2+}$ phosphor produced a diode emitting white light with ultra-wideband emission and a correlated color temperature of 4124 K. Overall, results indicated that the prepared samples may be potentially applied in white-light-emitting diodes.

1. Introduction

In recent years, white-light-emitting diodes (WLED) have received much attention because of their long lifetime, high production efficiency, good material stability, and efficient energy consumption.[1–3] Combination of cerium doped yttrium aluminum garnet (YAG) phosphor with blue InGaN chips is a common method to generate WLED. However, the lack of red-light contribution in this method limits its applications.[4,5] This limitation may be solved by using an ultraviolet light-emitting diodes (LED) chip coated with three phosphors emitting blue, green, and red light. In this WLED system, the blue emission efficiency is usually poor because of the strong reabsorption.[6] Hence, single-composition white-emitting phosphors for ultraviolet (UV) or near-ultraviolet (NUV) excitations have gained much attention for solid-state lighting. Single-composition white phosphors with UV/NUV chips exhibit excellent color rendering index and color stability compared with YAG-based system.[7,8] A common method for producing white light with single-phased phosphors is by co-doping sensitizers and activators into the same crystalline matrix.[9] White light is generated by different activators or by one type of activators at different sites in a single host matrix.[10] Thus, selecting suitable activators and proper host matrix is crucial to generate white light.

Eu^{2+} and Ce^{3+} are two important activators that have been widely investigated for LED applications.[11–15] The 5d states of Ce^{3+} and Eu^{2+} are outer orbitals, and the coordination surroundings significantly affect the energies of these ions. Thus, emissions arising from 5d–4f electronic transitions are wavelength tunable because they are sensitive to crystal-field splitting and nephelauxetic effects. These characteristics of Ce^{3+} and Eu^{2+} ions enable them to own the ability of facilitating white-light-emission.

However, to the best of our knowledge, till now few white-light-emitting phosphors based on the combinations of the luminescence of Ce^{3+} and Eu^{2+} in a single phosphate host have been reported, which is mainly due to that it's hard for Ce^{3+} and Eu^{2+} to achieve blue green and red emissions simultaneously in a single oxide host. The Eu^{2+}-doped $Ca_4(PO_4)_2O$ red emission phosphor with excellent optical properties was firstly discovered by our work group.[16] Our present work aims to develop a new single-phased white-light-emitting phosphor by using Ce^{3+} and Eu^{2+} ions as activators. Ce^{3+} ions can function as a good sensitizer and previous studies reported the energy transfer phenomenon in single-component phosphors, such as $Sr_3B_2O_6:Ce^{3+},Eu^{2+}$ and $Ca_2PO_4Cl:Ce^{3+}$, Eu^{2+}.[17-19] Based on the energy transfer mechanism, a novel single-composition $Ca_4(PO_4)_2O:Ce^{3+},Eu^{2+}$ phosphor emitting white light was obtained. The luminescent properties and energy transfer process between the sensitizer Ce^{3+} and activator Eu^{2+} were investigated, and the phosphor has excellent Color Rendering Index and wide spectral distribution.

2. Experimental Section

2.1 Materials and Synthesis

A series of powder samples of $Ca_4(PO_4)_2O$:xCe^{3+},yEu^{2+} (x = 0–0.045, y = 0–0.14) was prepared through high-temperature solid-state method with $CaCO_3$ (A.R), $CaHPO_4$ (A.R.), CeO_2 (99.99%), and Eu_2O_3 (99.99%). The stoichiometric amount of raw materials was thoroughly ground in an agate mortar. The homogeneous mixture was transferred into an alumina crucible and then heated at 1693 K for 6 h in CO atmosphere.

2.2 Materials Characterization

Powder X-ray diffraction (XRD) measurements were performed on a Bruker D8 focus diffractometer with graphite-monochromatized Cu Kα radiation (λ = 0.15405 nm) operating at 40 kV and 40 mA. Rietveld refinements on the XRD data were performed using the software GSAS. The elemental analysis was performed through Inductively Coupled Plasma Optical Emission Spectrometer (ICP-OES). The diffuse reflectance spectra were recorded using a 3600 UV-VIS-NIR spectrophotometer, with barium sulfate as the reference. Photoluminescence emission (PL) and photoluminescence excitation (PLE) spectra were recorded using a Hitachi F-7000 spectrophotometer equipped with a 150-W xenon lamp under a working voltage of 700 V. The phosphors were thoroughly ground in an agate mortar, and the powders were put into sample cell, which was fixed by a cell holder for measurement. The excitation and emission slits were both set at 2.5 nm. The fluorescence decay curves were obtained using a Lecroy Wave Runner 6100 Digital Oscilloscope (1GHz), with a tunable laser (pulse width = 4 ns; gate = 50 ns) as the excitation source. The temperature-dependent PL properties of the phosphors were recorded using an FLS-920-combined fluorescence lifetime and steady-state spectrometer (Edinburgh Instruments) with a 450-W xenon lamp as the excitation source.

3. Results and Discussion

3.1 Phase identification and crystal Structure

Powder XRD was performed to verify the phase purity of the samples. Figure 1a shows the representative XRD patterns of the prepared samples. All diffraction peaks can be basically indexed to the standard data of $Ca_4(PO_4)_2O$ (JCPDS no. 25-1137), indicating that Eu^{2+} and Ce^{3+} ions were successfully incorporated into the $Ca_4(PO_4)_2O$ host lattice without inducing significant changes in the crystal structure. The elemental analysis was performed through ICP-OES. In the $Ca_4(PO_4)_2O$:0.02Ce^{3+},0.01Eu^{2+} phosphor, the mole ratio of Ca, P, Ce and Eu is 3.968 : 1.987 : 0.019 : 0.009. The results are consistent with the ratio of starting reagents.

The Rietveld refinements of the XRD data profiles of $Ca_4(PO_4)_2O$:0.02Ce^{3+},0.01Eu^{2+} are shown in Figure 2a, which presents detailed crystal information regarding the prepared samples. The results imply that $Ca_4(PO_4)_2O$:0.02Ce^{3+},0.01Eu^{2+} crystallizes in a monoclinic unit cell with the space group $P2_1$. The parameters included a = 7.014 Å, b = 11.978 Å, c = 9.465 Å, β = 90.87°, and V = 795.16 Å^3. The refinement finally converged to the goodness of fit coefficient with R_p = 7.56%, R_{wp} = 9.93%, and χ^2 = 1.55, as shown in Table 1.

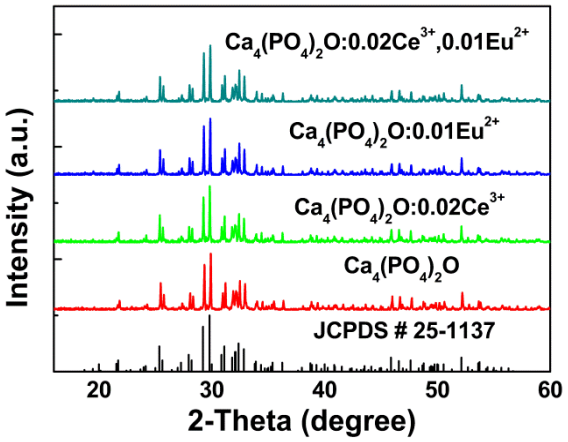

Figure 1. (a) XRD patterns of the typical prepared phosphors. The standard data for $Ca_4(PO_4)_2O$ (JCPDS 25-1137) is shown as references.

Table 1. Structural parameters for $Ca_4(PO_4)_2O$:0.02Ce^{3+},0.01Eu^{2+} as determined by Rietveld refinement of the powder XRD data at room temperature.

Formula	*$Ca_4(PO_4)_2O$:0.02Ce^{3+},0.01Eu^{2+}*
Space group	$P2_1$ – monoclinic
Units, Z	4
a (Å)	7.014
b (Å)	11.978
c (Å)	9.465
β	90.87
V (Å^3)	795.16
R_p (%)	7.56
R_{wp} (%)	9.93
χ^2	1.55

The crystal structure of $Ca_4(PO_4)_2O$ is simulated and shown in Figure 2b. Eight crystallographic sites, including Ca(1) to Ca(8), exist in the crystal lattice in the unit cell of $Ca_4(PO_4)_2O$.[20] The coordination for Ca(6) site is eight, whereas that for the other calcium sites is seven. The coordination geometry for Ca(1), Ca(3), Ca(4), Ca(5), and Ca(8) sites is approximately pentagonal bipyramid, whereas the coordination polyhedron for Ca(2), Ca(6), and Ca(7) is irregular. These polyhedrons connect to one another through four types of PO_4 groups and two types of unique oxygen atoms. Each unique oxygen atom is strongly coordinated to the calcium atoms, and the O–Ca distances for unique oxygen atoms are smaller than those connected with the PO_4 groups. Remarkably, the ionic radii for the seven- and eight-coordinated Ca^{2+} ions are 1.06 and 1.12 Å, respectively. The ionic radii for the seven- and eight-coordinated Eu^{2+} ions are 1.2 and 1.25 Å, whereas that for the seven and eight-coordinated Ce^{3+} ions are 1.07 and 1.143 Å. Hence, Eu^{2+} and Ce^{3+} can efficiently substitute Ca^{2+} ions because of their similar ionic radii.

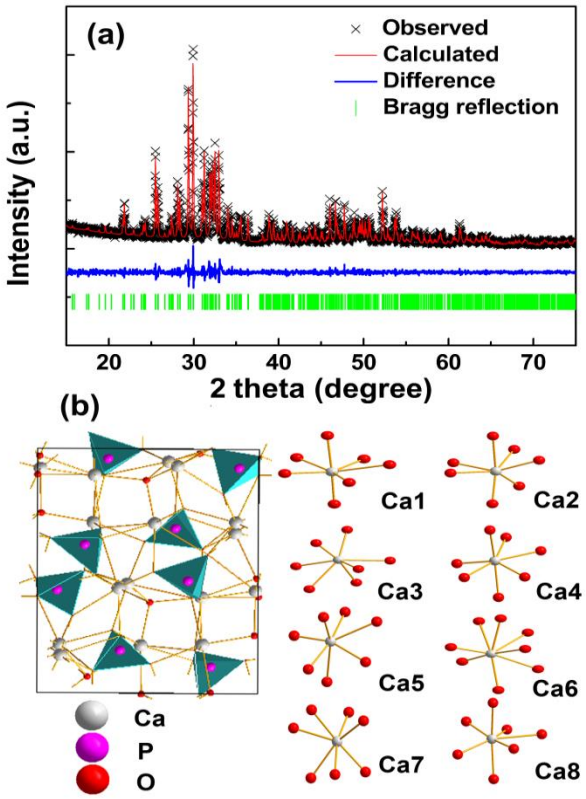

Figure 2. (a) Observed (cross), calculated (red) , and difference results (blue) of powder X-ray diffraction refinement of $Ca_4(PO_4)_2O$:0.02Ce^{3+},0.01Eu^{2+}. (b) Crystal structure diagram of $Ca_4(PO_4)_2O$.

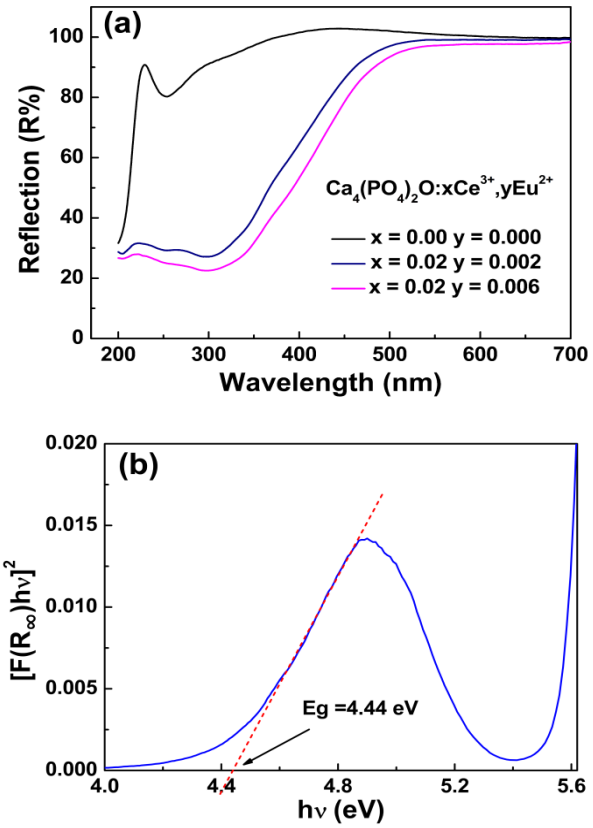

Figure 3. (a) Diffuse reflectance spectra of $Ca_4(PO_4)_2O$:xCe^{3+},yEu^{2+} (x = 0–0.02, y = 0–0.05). (b) $h\nu$ - $[h\nu F(R_\infty)]^2$ curve of $Ca_4(PO_4)_2O$.

3.2 Diffuse Reflectance Spectra of $Ca_4(PO_4)_2O:Ce^{3+},Eu^{2+}$

The reflectance spectra of several samples are shown in Figure 3a. The $Ca_4(PO_4)_2O$ host material shows an energy absorption band around 250 nm. As Ce^{3+} ions were doped into the $Ca_4(PO_4)_2O$ host, a strong broad absorption appeared in the 250–400 nm NUV range; this band is ascribed to the $4f^1$–$5d^1$ absorption of Ce^{3+} ions. For the $Ca_4(PO_4)_2O$ samples co-doped with Ce^{3+} and Eu^{2+}, the absorption edges gradually extend to long wavelengths and absorption is enhanced for high Ce^{3+} and Eu^{2+} ion concentration. As a result, the excitation wavelength presents an overall red shift to 450 nm, which matches well with NUV chips for applications in white-light NUV LEDs.

The band gap of the $Ca_4(PO_4)_2O$ host can be estimated using the following formula:[21]

$$[F(R_\infty)h\nu]^n = A(h\nu - E_g) \quad (1)$$

where h is the Planck's constant, ν is the frequency of vibration, E_g is the value of band gap, A is the proportional constant, n = 2 denotes the direct allowed transition. $F(R_\infty)$ is the Kubelka–Munk absorption coefficient calculated from the measured reflectance (R) through the following relationship:[22]

$$F(R_\infty) = (1 - R^2)/2R \quad (2)$$

Using the Kubelka–Munk function, $(h\nu F(R_\infty))^2$ is plotted against $h\nu$ as shown in Figure 3b. E_g is approximately 4.44 eV.

3.3 Photoluminescence Properties of $Ca_4(PO_4)_2O:Ce^{3+}$ Phosphors

Figure 4a shows the PLE and PL spectra of the $Ca_4(PO_4)_2O$:0.02Ce^{3+} phosphor. The PLE spectrum exhibits a broad absorption from 260 nm to 430 nm that originates from $4f^1$–$5d^1$ transition of Ce^{3+} ions; this broad absorption matches well with the InGaN-based LED. This finding indicates the potential application of the phosphor for WLED. Under the excitation of 380 nm, the $Ca_4(PO_4)_2O$:0.02Ce^{3+} phosphor exhibits intense blue emission caused by the 5d–4f electronic dipole-allowed transition of Ce^{3+}; this emission consists of a strong asymmetric broad band (400–600 nm) with a maximum at 453 nm. The emission spectra of Ce^{3+} should contain two sub-bands caused by the spin-orbit splitting of the ground state ($^2F_{5/2}$ and $^2F_{7/2}$) with an energy difference of approximately 2000 cm^{-1}.[23,24] Figure 4b presents the asymmetric emission band that can be decomposed into two well-separated Gaussian components with maxima at 440 and 480 nm. The energy difference between 440 and 480 nm is 1894 cm^{-1}, which is almost in agreement with the reported value of 2000 cm^{-1}. Eight Ca^{2+} crystallographic sites exist in the crystal structure, and any types of Ca^{2+} may be substituted by Ce^{3+} ions. However, one type of luminescence center is inconsistent with this result. One possible explanation is the similarity of the crystal-field environments even though the coordination environment of the Ca^{2+} crystallographic sites differs.

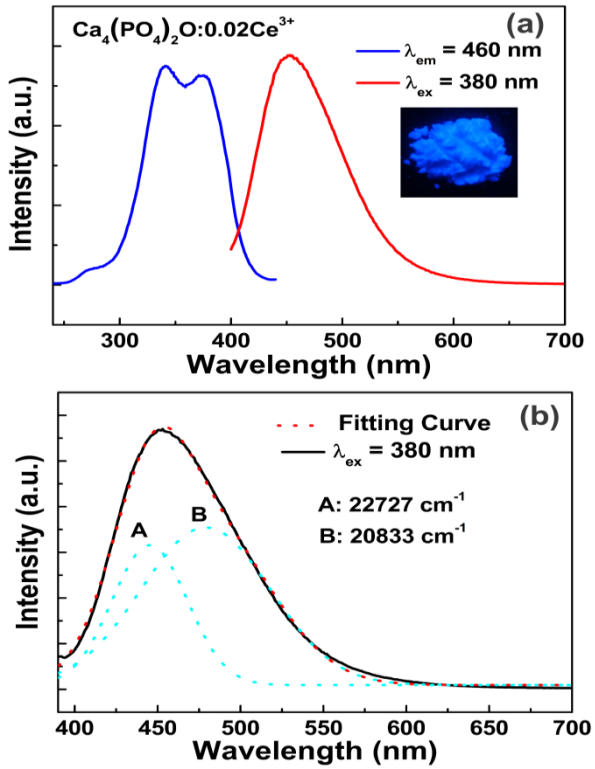

Figure 4. (a) PL and PLE spectra of $Ca_4(PO_4)_2O:0.02Ce^{3+}$. (b) The deconvoluted emission spectrum of $Ca_4(PO_4)_2O:0.02Ce^{3+}$ as the sum of two Gaussian components.

Figure 5 shows the relative emission spectra as a function of Ce^{3+} concentration (x). The PL intensity of Ce^{3+} increases with its increasing concentration (x); the intensity reaches a maximum value at x = 0.02 and then decreases with further augment of its concentration (x) because of the concentration quenching effect. Hence, we calculated the critical distance between Ce^{3+} ions for concentration quenching by using the following equation:[25]

$$R_c \approx 2\left[\frac{3V}{4\pi x_c Z}\right]^{1/3} \qquad (3)$$

where V is the volume of the unit cell, x_c is the critical concentration of activator, and Z is the number of formula units per unit cell. For the $Ca_4(PO_4)_2O$ host, the calculated R_c is 26.27 Å when Z = 4, x_c = 0.02, and V = 795.16 Å^3 are used. However, the exchange interaction generally occurs in a forbidden transition (R_c is typically 5 Å).[11] Therefore, energy transfer does not belong to exchange interactions but to electric multipole–multipole interactions. Thus, the optimum doping concentration for Ce^{3+} is 2 mol% in the $Ca_4(PO_4)_2O$ host.

3.4 Photoluminescence Properties of $Ca_4(PO_4)_2O:Eu^{2+}$

The PL and PLE spectra of $Ca_4(PO_4)_2O:0.07Eu^{2+}$ are shown in Figure 6a. The PLE spectrum demonstrates a broad absorption that covers the whole UV and blue regions from 300–550 nm with a maximum at 460 nm. $Ca_4(PO_4)_2O:0.07Eu^{2+}$ shows a strong broad band red emission from 550 nm to 800 nm with a

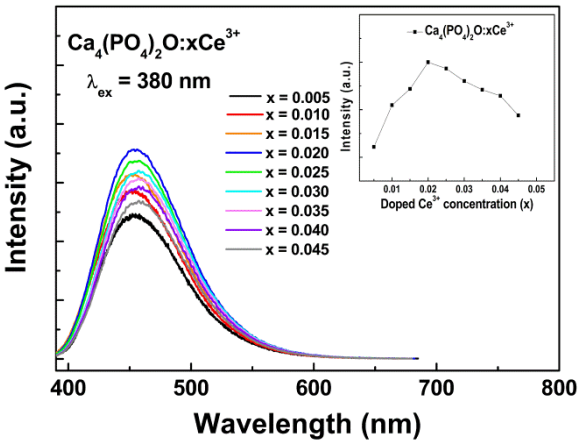

Figure 5. PL spectra of $Ca_4(PO_4)_2O:xCe^{3+}$ (x = 0.005–0.045), the inset shows the integrated intensity as a function of Ce^{3+} concentration.

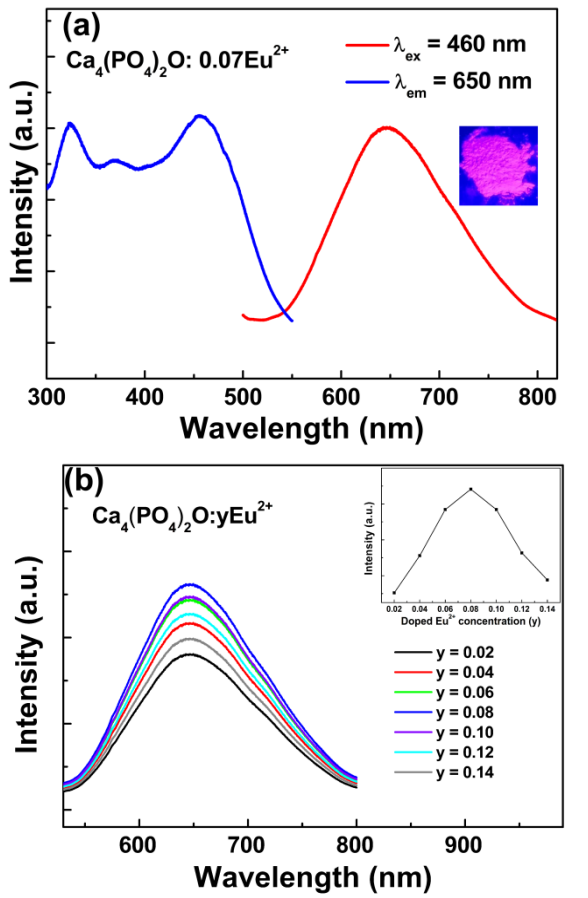

Figure 6. (a) PL and PLE spectra of $Ca_4(PO_4)_2O:0.07Eu^{2+}$. The inset shows phosphor photograph excited at 460 nm. (b) PL intensity of $Ca_4(PO_4)_2O:yEu^{2+}$ (y = 0–0.14) phosphors as a function of Eu^{2+} concentration.

maximum at 650 nm under 460 nm excitation; this band can be attributed to the $4f^65d^1 \rightarrow 4f^7$ allowed transition of Eu^{2+}.[26]

The energies of the spin- and dipole-allowed transitions from the $4f^7$ ground state to the $4f^65d^1$ excited state of the lanthanides are lower than those of the free ion value when the ions are placed in a crystalline environment. The crystallographic

structure dependence of the emission position of Eu^{2+} can be mainly determined through the nephelauxetic effect and crystal-field splitting of the $5d^1$ configuration. For divalent and some trivalent rare earth ions in suitable materials, emission may occur from the low energy edge of the d-band.

The position of the d-band edge (E) and emission peak position can be estimated through the following equation:[27]

$$E = Q\left[1 - (V/4)^{1/V} 10^{-nE_a r/80}\right] \quad (4)$$

where Q is the position of energy for the lower d-band edge for the free rare earth ion, V is the valence of the active cationic ions, E_a is the electron affinity of the atoms that form anions, n is the coordination number of the active ion, and r is the radius of the host cation replaced by rare earth ions. For $Ca_4(PO_4)_2O:Eu^{2+}$, Q = 34000 cm^{-1}, E_a = 1.17 eV for oxygen atoms, V = 2, r = 1.06 Å for n = 7 and r = 1.12 Å for n = 8. The obtained E value is 15273.9 cm^{-1} (654.7 nm) for n = 7 and 16220.3 cm^{-1} (616.5 nm) for n = 8. These calculated results are inconsistent with the emission properties of $Ca_4(PO_4)_2O:0.07Eu^{2+}$. The emission spectrum of $Ca_4(PO_4)_2O:0.07Eu^{2+}$ contains only one broad band centered at approximately 650 nm; this band may be ascribed to the emission of the luminescence center of the seven-coordinated Eu^{2+}. The Ca(6) site is surrounded by eight oxygen atoms but also includes an oxygen atom with large Ca–O distance (2.996 Å), implying that the coordination influence from this oxygen atom is weak for Eu^{2+} ions. Therefore, this phenomenon can be attributed to the similarity of the crystal-field environments even if the coordination numbers of the Ca^{2+} crystallography sites differ.

Figure 6b shows the relative emission intensity as a function of Eu^{2+} concentration (y). Initially, the PL intensity increases with increased Eu^{2+} concentration (y), reaches a maximum value at x = 0.08, and then decreases with further augment of its concentration (y) because of the concentration quenching effect. As a result, the critical energy transfer distances between Eu^{2+} ions in the phosphor can be calculated using equation (3). The calculated R_c is 16.81 Å. In addition, the exchange interaction occurs when the distance between the activators is shorter than 5 Å.[11] Therefore, the multipole–multipole interaction dominates the concentration quenching mechanism of Eu^{2+} emission.

3.5 Photoluminescence Properties and Energy Transfer in $Ca_4(PO_4)_2O:Ce^{3+},Eu^{2+}$ Samples

An essential condition of energy transfer is the overlap between the donor emission and the acceptor excitation spectra. Figure 7 clearly presents a significant spectral overlap between the emission band of Ce^{3+} and the excitation band of Eu^{2+}; hence, the energy transfer from Ce^{3+} to Eu^{2+} occurs. Figure 7c also shows the PLE and PL spectra of $Ca_4(PO_4)_2O:0.02Ce^{3+},0.012Eu^{2+}$. The black solid line monitored at 650 nm exhibits a combined PLE spectrum of Ce^{3+} and Eu^{2+}. This result demonstrates an efficient energy transfer from Ce^{3+} to Eu^{2+}.

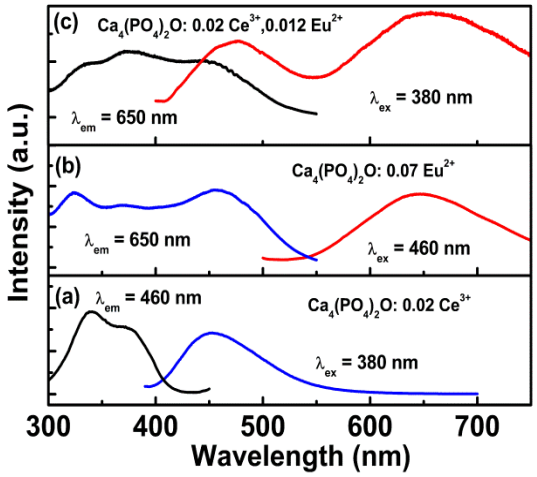

Figure 7. PL and PLE spectra of $Ca_4(PO_4)_2O:0.02Ce^{3+}$ (a), $Ca_4(PO_4)_2O:0.07Eu^{2+}$ (b), $Ca_4(PO_4)_2O:0.02\ Ce^{3+},0.012Eu^{2+}$ (c).

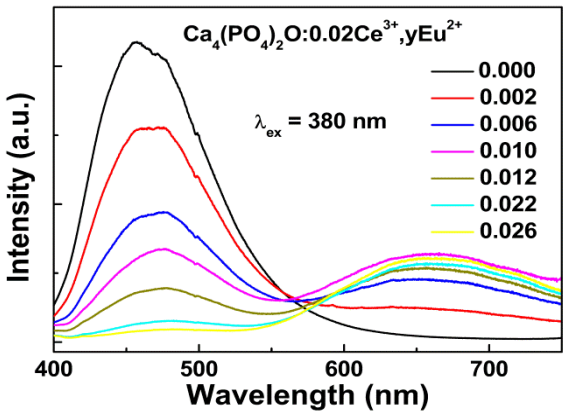

Figure 8. PL spectra of a series of $Ca_4(PO_4)_2O:0.02Ce^{3+},yEu^{2+}$ phosphors (y = 0, 0.002, 0.006, 0.010, 0.012, 0.022, and 0.026) excited at 380 nm.

Figure 8 shows the emission spectra of $Ca_4(PO_4)_2O:0.02Ce^{3+},yEu^{2+}$ (y = 0–0.026). The PL spectra of $Ca_4(PO_4)_2O:0.02Ce^{3+},yEu^{2+}$ contains a broad blue emission band and a red emission band under excitation at 380 nm. The broad emission band from 400 nm to 550 nm is ascribed to the allowed f–d transition of the Ce^{3+}, whereas the emission band centered at 650 nm is attributed to the f–d transition of the Eu^{2+}. The intensity of the red emission at 650 nm reaches the maximum at y = 0.01 and then decreases because of concentration quenching.[28]. These results indicate that the occurrence of energy transfer from Ce^{3+} to Eu^{2+} ions.

To further validate the energy transfer from Ce^{3+} to Eu^{2+}, we investigated the decay curves of $Ca_4(PO_4)_2O:0.02Ce^{3+},yEu^{2+}$ (y = 0–0.012) with excitation at 380 nm and monitored at 460 nm. Figure 9a shows the representative decay curves of Ce^{3+} emission in the $Ca_4(PO_4)_2O:0.02Ce^{3+},yEu^{2+}$ (y = 0.000, 0.012) samples.

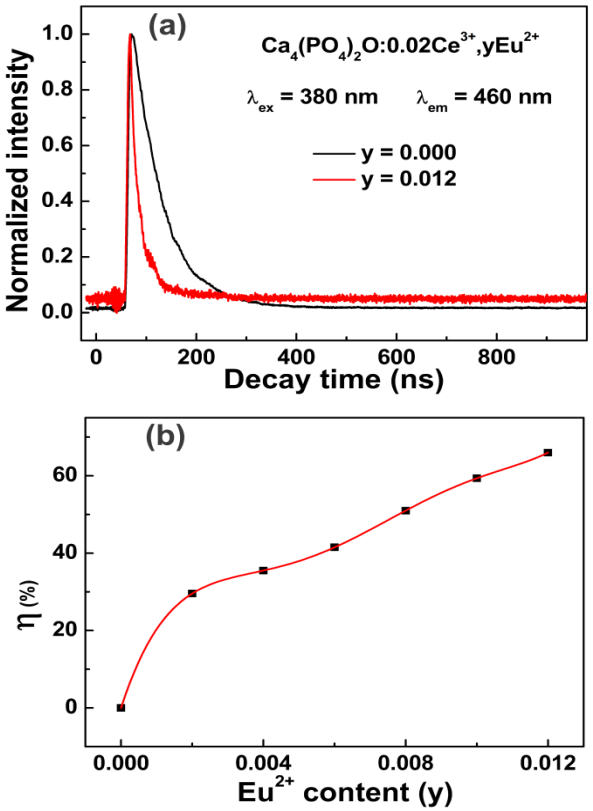

Figure 9. (a) Decay curves of Ce^{3+} emission in $Ca_4(PO_4)_2O:0.02Ce^{3+},yEu^{2+}$ (y =0, 0.002, 0.006, 0.010, 0.012, 0.022, and 0.026) samples excited at 380 nm and monitored at 460 nm. (b) Energy transfer efficiencies from Ce^{3+} to Eu^{2+} in $Ca_4(PO_4)_2O:0.02Ce^{3+},yEu^{2+}$ (y = 0–0.012) samples.

The decay curve of $Ca_4(PO_4)_2O:0.02Ce^{3+}$ was analyzed using curve fitting and can be well-fitted through a single-exponential function:

$$I = I_0 \exp(^{-t}/_{\tau}) \quad (5)$$

where I_0 and I are the luminescence intensities at time 0 and t, respectively, and τ is the decay lifetime. For the $Ca_4(PO_4)_2O:0.02Ce^{3+}$ sample, the lifetime values of τ are 59.9 ns. For the Ce^{3+} and Eu^{2+} co-doped samples, the fluorescence decay presents slight inconformity with a single-exponential function. An effective lifetime can be defined as:[29]

$$\tau = \frac{\int_0^\infty tI(t)dt}{\int_0^\infty I(t)dt} \quad (6)$$

This equation was used to calculate decay times. The corresponding decay times were 42.2, 35.0, 24.3, 20.2, 18.0, and 15.2 ns for the $Ca_4(PO_4)_2O:0.02Ce^{3+},yEu^{2+}$ phosphors with y = 0.002, 0.004, 0.006, 0.008, 0.010, and 0.012, respectively. The decay lifetime of Ce^{3+} ions decreases with increased Eu^{2+} doping content. This finding strongly confirms the existence of energy transfer from Ce^{3+} to Eu^{2+} ions. The energy transfer efficiency from Ce^{3+} to Eu^{2+} ions can be expressed by the following equation:[30,31]

$$\eta_T = 1 - \frac{\tau_S}{\tau_{S_0}} \quad (7)$$

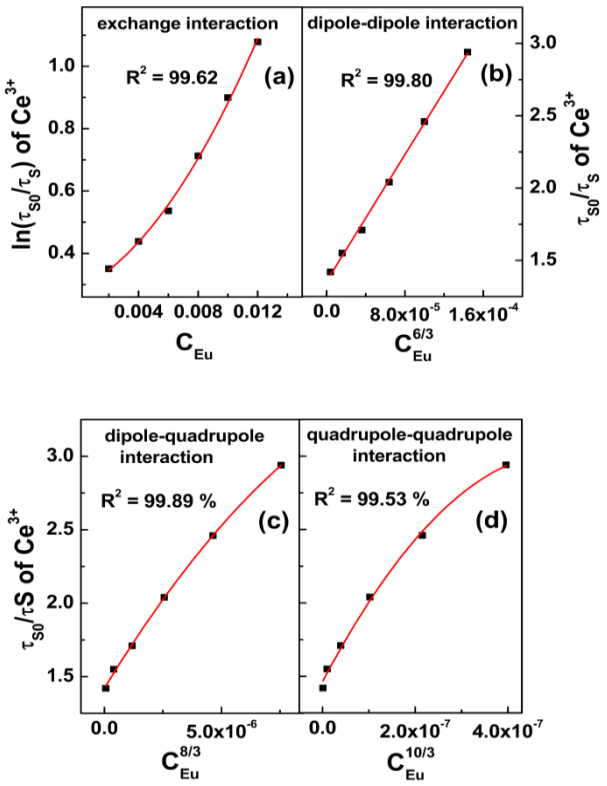

Figure 10. Dependence of $\ln(\tau_{S0}/\tau_S)$ of Ce^{3+} on C (a) and τ_{S0}/τ_S of Ce^{3+} on $C^{6/3}$ (b), $C^{8/3}$ (c) and $C^{10/3}$ (d).

where η_T is the energy transfer efficiency, and τ_{S_0} and τ_S are the lifetimes of the Ce^{3+} sensitizer in the absence and presence of Eu^{2+} ions, respectively. The η_T values of the $Ca_4(PO_4)_2O:0.02Ce^{3+},yEu^{2+}$ samples were calculated as a function of Eu^{2+} concentration (y), and the results are shown in Figure 9b. The value of η_T increases with increasing Eu^{2+} concentration, but the increscent rate of the energy transfer efficiency gradually decreases with the augment of Eu^{2+} concentration. The maximum energy transfer efficiency reaches 65% when y = 0.012. These results indicate that the energy transfer from Ce^{3+} to Eu^{2+} is highly effective.

According to Dexter's energy transfer formula of multipolar interaction and Reisfeld's approximation, the following relationship can be obtained:[23]

$$\ln\left(\frac{\tau_{S_0}}{\tau_S}\right) = C \quad (8)$$

$$\frac{\tau_{S_0}}{\tau_S} \propto C^{n/3} \quad (9)$$

where C is the doping concentration of Eu^{2+} ions. Equation (8) corresponds to the exchange interaction, and Equation (9) with n = 6, 8, 10 corresponds to dipole–dipole, dipole–quadrupole, and quadrupole–quadrupole interactions, respectively.

The relationship of $\ln(\tau_{S0}/\tau_S) - C$ and $\tau_{S0}/\tau_S - C^{n/3}$ plots are illustrated in Figure 10, and a linear relationship can be observed when n = 6. This finding clearly indicates that the energy transfer from Ce^{3+} to Eu^{2+} occurs via a dipole–dipole

mechanism. For the electric dipole–dipole mechanism, the critical distance (R_c) for energy transfer from Ce^{3+} to Eu^{2+} can be calculated using the formula:[29]

$$R_c^6 = 3 \times 10^{12} f_d \int \frac{F_S(E)F_A(E)}{E^4} dE \quad (10)$$

where f_d = 0.02 is the electric dipole oscillator strength for Eu^{2+} ions. $\int F_S(E)F_A(E)/E^4 dE$ represents the spectral overlap between the normalized shapes of Ce^{3+} emission $F_S(E)$ and Eu^{2+} excitation $F_A(E)$ and is calculated as 0.00756. The obtained R_c is 27.7 Å. Furthermore, the critical distance was also estimated according to Equation (3). In the $Ca_4(PO_4)_2O$:0.02Ce^{3+},yEu^{2+} samples, the critical concentration can be obtained when the energy transfer efficiency η_T is 0.5. R_c was estimated as 23.8 Å through concentration quenching method. This result is consistent with the findings obtained using spectral overlap method. Hence, the energy transfer from Ce^{3+} to Eu^{2+} ions is mainly ascribed to the dipole–dipole interaction. On the basis of the spectra and energy transfer, we propose an energy level scheme for Ce^{3+} and Eu^{2+} in $Ca_4(PO_4)_2O$ as illustrated in Figure 11.

The CIE chromaticity coordinates of $Ca_4(PO_4)_2O$:0.02Ce^{3+},yEu^{2+} (y = 0, 0.002, 0.006, 0.010, 0.012, 0.022, 0.026) under the excitation of 380 nm are shown in Figure 12. Energy transfer can produce white light in a single host because of the multiplex light of Ce^{3+} and Eu^{2+} ions. With increasing Eu^{2+} content, the CIE chromaticity coordinates systematically change from (0.165, 0.188) to (0.519, 0.366). The corresponding color tone of samples gradually changes from blue to white and eventually to orange. Therefore, white light can be obtained by adjusting the proportion of Eu^{2+} and Ce^{3+} to satisfy the requirements of different illumination applications.

3.6 Thermal Stability and LED Component by NUV Chip

Thermal stability of phosphors is important for high-power LED applications. The temperature dependence of emission intensity for the $Ca_4(PO_4)_2O$:0.02Ce^{3+},0.012Eu^{2+} phosphor under 380 nm excitation is shown in Figure 13. The relative emission intensity decreases with increased temperature from 295 K to 473 K. The activation energy (E_a) can be expressed with the formula:[32]

$$I = \frac{I_0}{1 + c\ exp\left(-\frac{E_a}{kT}\right)} \quad (11)$$

where I_o and I are the luminescence intensities of the $Ca_4(PO_4)_2O$:Ce^{3+},Eu^{2+} phosphor at room temperature and testing temperature, respectively, E_a represents the thermal quenching activation energy of the phosphor, c is the rate constant for thermally activated escape (constant for the same loss), and k is the Boltzmann constant (8.629×10^{-5} eV/K). Figure 13 presents the plots of ln[(I_0/I)-1] versus 1/T for $Ca_4(PO_4)_2O$:0.02Ce^{3+},0.012Eu^{2+}. The calculated E_a is 0.1397 eV for the phosphor, which is higher than that of recently reported phosphors.[28,33]

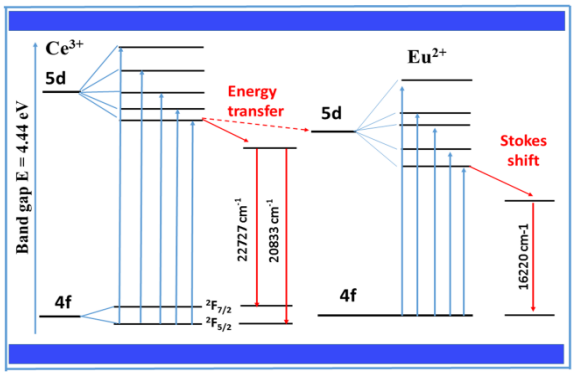

Figure 11. Schematic energy structure of Ce 4f and 5d levels in $Ca_4(PO_4)_2O$:Ce^{3+},Eu^{2+}. Numbers shown over the arrows denote the corresponding transition energies in cm^{-1}.

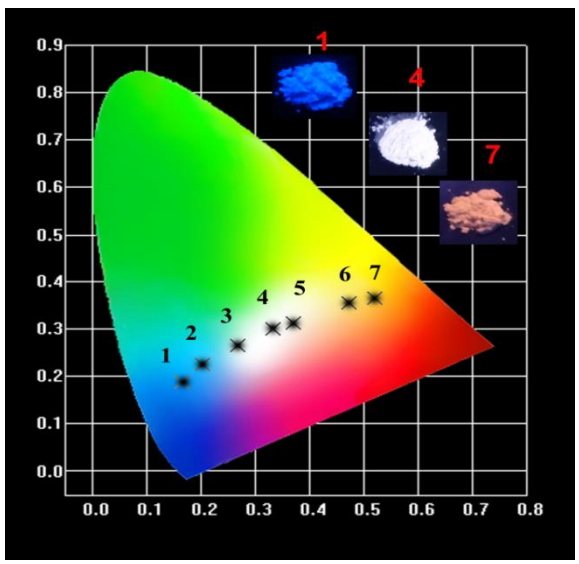

Figure 12. CIE coordinates of $Ca_4(PO_4)_2O$:0.02Ce^{3+},yEu^{2+} phosphors (y = 0, 0.002, 0.006, 0.010, 0.012, 0.022, and 0.026). Insets show the phosphor images with different Eu^{2+} doping concentrations excited at 380 nm.

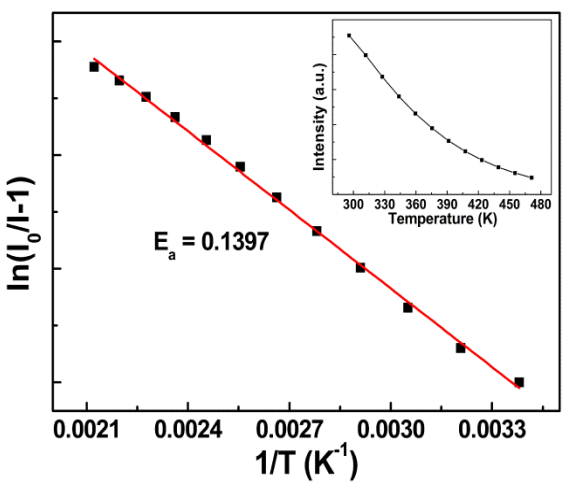

Figure 13. The activation energy of $Ca_4(PO_4)_2O$:0.02Ce^{3+},0.012Eu^{2+}phosphor, inset shows the plot of PL intensity versus temperature of $Ca_4(PO_4)_2O$:0.02Ce^{3+},0.012Eu^{2+}.

The temperature-dependent emission spectra of $Ca_4(PO_4)_2O:Ce^{3+}$ and $Ca_4(PO_4)_2O:Eu^{2+}$ should also be considered because of the different quenching rates of Ce^{3+} and Eu^{2+} emissions. Figures 14a and 14b show the temperature-dependent emission spectra of the $Ca_4(PO_4)_2O:0.02Ce^{3+}$ and $Ca_4(PO_4)_2O:0.012Eu^{2+}$ samples. The profiles of the emission spectra for the two samples remain constant even if the temperature increases (T = 293−443 K). The temperature-dependent integrated luminescence intensities of $Ca_4(PO_4)_2O:0.02Ce^{3+}$ and $Ca_4(PO_4)_2O:0.012Eu^{2+}$ are shown in Figure 14c. Hence, the $Ca_4(PO_4)_2O:0.02Ce^{3+}$ phosphors exhibit higher thermal stability than the $Ca_4(PO_4)_2O:0.012Eu^{2+}$ phosphors. The color coordinates of Ce^{3+} and Eu^{2+} co-doped phosphors vary with different temperatures. Figure 15 shows the selected temperature-dependent emission spectra and the color coordinate of $Ca_4(PO_4)_2O:0.02Ce^{3+},0.012Eu^{2+}$. The profiles of the emission spectra of the phosphor exhibit minimal changes with increasing temperature (T = 293−413 K) as demonstrated in Figure 15a. However, Figure 15b shows that the phosphor also emits white light with the temperature increasing up to 413 K.

Figure 16 shows the electroluminescence spectrum of WLED lamp fabricated using a NUV 380 nm chip combined with $Ca_4(PO_4)_2O:0.02Ce^{3+},0.012Eu^{2+}$ phosphor and stimulated with 700-mA current. The WLED lamp package emits intense warm white light with a correlated color temperature of 4124 K and a color coordinate of (0.359, 0.310). The value of R_a is 84, which is higher than that (R_a = 78) of an WLED based on YAG:Ce with a blue InGaN chip. These results indicate that $Ca_4(PO_4)_2O:Ce^{3+},Eu^{2+}$ is a potential single-composition phosphor for WLED applications.

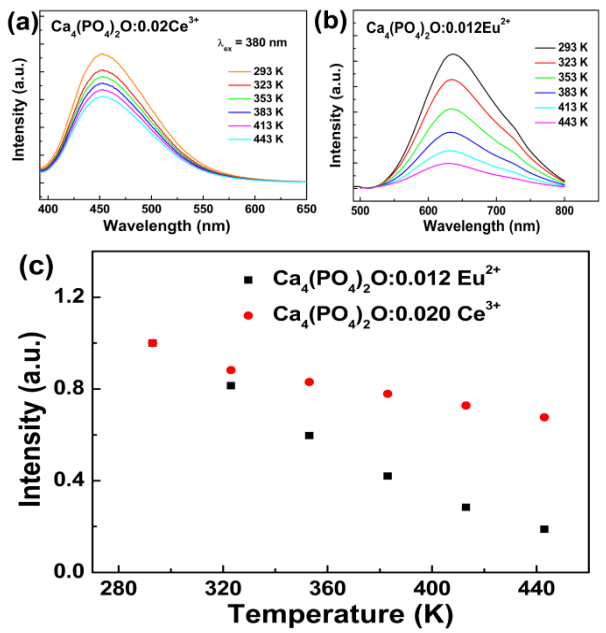

Figure 14. Temperature-dependent emission spectra of $Ca_4(PO_4)_2O:0.02\ Ce^{3+}$ and $Ca_4(PO_4)_2O:0.012Eu^{2+}$ samples (a, b). Temperature-dependent integrated luminescence intensities of $Ca_4(PO_4)_2O:0.02\ Ce^{3+}$ and $Ca_4(PO_4)_2O:0.012Eu^{2+}$ (c).

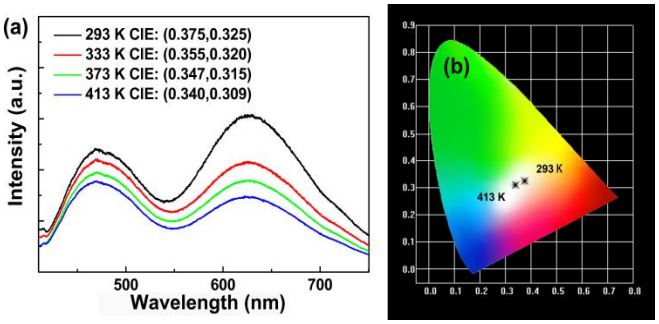

Figure 15. (a) Selected temperature-dependent emission spectra of $Ca_4(PO_4)_2O:0.02Ce^{3+},0.012Eu^{2+}$. (b) CIE chromaticity diagram of phosphor.

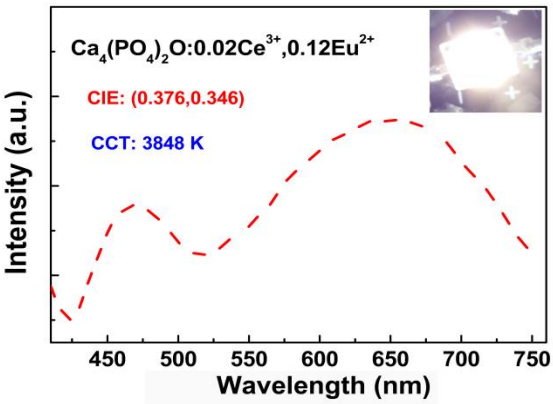

Figure 16. Electroluminescence spectrum of $Ca_4(PO_4)_2O:0.02Ce^{3+},0.012Eu^{2+}$ phosphor-based WLED under a current of 700 mA. The inset shows a photograph of the LED package.

4. Conclusion

A novel color-tunable and single-composition NUV LED phosphor emitting white light was synthesized through solid-state reaction method. A wide-ranged tunable blue–white–orange emission is obtained by precisely controlling the ratio of Ce^{3+} to Eu^{2+}. The energy transfer from Ce^{3+} to Eu^{2+} in the $Ca_4(PO_4)_2O$ host is a resonant type via electric dipole–dipole mechanism. The energy structure levels of $Ca_4(PO_4)_2O:Ce^{3+},Eu^{2+}$ and the transition paths were also analyzed. A WLED device was fabricated through the combination of a NUV 380-nm chip and the $Ca_4(PO_4)_2O:0.02Ce^{3+},0.012Eu^{2+}$ phosphor. This device emits an intense warm white light with a low correlated color temperature (4124 K).

Acknowledgments

This research is financially supported by Hong Kong, Macao and Taiwan Science & Technology Cooperation Program of China (2014DFT10310). RSL would like to thank the Industrial Technology Research Institute (Contract No. D351A41300) and Ministry of Science and Technology of Taiwan (Contract No. MOST 101-2113-M-002-014-MY3) for financially supporting this work.

Notes and references

[a]State key Laboratory of Rare Earth Resource Utilization, Changchun Institute of Applied Chemistry, Chinese Academy of Sciences, Changchun 130022, P. R. China.
[b]University of Chinese Academy of Sciences, Beijing 100049, P. R. China.
[c]Department of Chemistry, National Taiwan University, Taipei 106, Taiwan.
[d]Department of Mechanical Engineering and Graduate Institute of Manufacturing Technology, National Taipei University of Technology, Taipei 10608, Taiwan.
*Corresponding authors:
E-mail: cyli@ciac.ac.cn and rsliu@ntu.edu.tw

1 C. Feldmann, T. Jüstel, C. R. Ronda and P. J. Schmidt, *Adv. Funct. Mater*., 2003, **13**, 511.
2 T. Jüstel, H. Nikol and C. Ronda, *Angew. Chem. Int. Ed.*, 1998, **37**, 3084.
3 K. ul Hasan, M. O. Sandberg, O. Nur and M. Willander, *Adv. Optical Mater*., 2014, **2**, 326.
4 X. Piao, T. Horikawa, H. Hanzawa and K.-i. Machida, *Appl. Phys. Lett.*, 2006, **88**, 161908.
5 H. S. Jang, Y. H. Won and D. Y. Jeon, *Appl. Phys. B*, 2009, **95**, 715.
6 Y.-S. Tang, S.-F. Hu, C. C. Lin, N. C. Bagkar and R.-S. Liu, *Appl. Phys. Lett.*, 2007, **90**, 151108.
7 J. Kido, H. Shionoya and K. Nagai, *Appl. Phys. Lett.*, 1995, **67**, 2281.
8 W. Lü, Z. Hao, X. Zhang, Y. Luo, X. Wang and J. Zhang, *Inorg. Chem.* 2011, **50**, 7846.
9 D. L. Dexter, *J. Chem. Phys.*, 1953, **21**, 836.
10 C. Guo, J. Yu, X. Ding, M. Li, Z. Ren and J. Bai, *J. Electrochem. Soc.*, 2011, **158**, J42.
11 W. B. Im, N. N. Fellows, S. P. DenBaars, R. Seshadri and Y.-I. Kim, *Chem. Mater*., 2009, **21**, 2957.
12 R.-J. Xie, N. Hirosaki, K. Sakuma, Y. Yamamoto and M. Mitomo, *Appl. Phys. Lett.*, 2004, **84**, 5404.
13 G. Blasse and G. J. Dirksen, *Phys. Status Solidi B*, 1982, **110**, 487.
14 D. Geng, M. Shang, Y. Zhang, H. Lian and J. Lin, *Dalton Trans.*, 2013, **42**, 15372.
15 C.-H. Huang and T.-M. Chen, *Inorg. Chem*., 2011, **50**, 5725.
16 R. P. Chengyu Li, Qiang Su, *ZL200710055669.0*, 2007.
17 C.-K. Chang and T.-M. Chen, *Appl. Phys. Lett.* , 2007, **91**, 081902.
18 Y. Song, G. Jia, M. Yang, Y. Huang, H. You and H. Zhang, *Appl. Phys. Lett.* 2009, **94**, 091902.
19 P. Li, Z. Wang, Z. Yang and Q. Guo, *RSC Adv.*, 2014, **4**, 27708.
20 B. Dickens, W. E. Brown, G. J. Kruger and J. M. Stewart, *Acta Crystallogr., Sect. B*, 1973, **29**, 2046.
21 Z. Jiang, Y. Wang and L. Wang, *J. Electrochem. Soc.*, 2010, **157**, J155.
22 Y.-I. Kim, K. Page, A. M. Limarga, D. R. Clarke and R. Seshadri, *Phys. Rev. B*, 2007, **76**, 115204.
23 M. Shang, G. Li, D. Geng, D. Yang, X. Kang, Y. Zhang, H. Lian and J. Lin, *J. Mater. Chem. C*, 2012, **116**, 10222-10231.
24 G. Blasse, *Chem. Mater.*, 1994, **6**, 1465.
25 N. Guo, Y. Huang, H. You, M. Yang, Y. Song, K. Liu and Y. Zheng, *Inorg. Chem.*, 2010, **49**, 10907.
26 D. Deng, H. Yu, Y. Li, Y. Hua, G. Jia, S. Zhao, H. Wang, L. Huang, Y. Li, C. Li and S. Xu, *J. Mater. Chem. C*, 2013, **1**, 3194.
27 L. G. van Uitert, *J. Lumin.*, 1984, **29**, 1.
28. W.-R. Liu, C.-H. Huang, C.-W. Yeh, J.-C. Tsai, Y.-C. Chiu, Y.-T. Yeh and R.-S. Liu, *Inorg. Chem.*, 2012, **51**, 9636.
29. Y. Jia, H. Qiao, Y. Zheng, N. Guo and H. You, *Phys. Chem. Chem. Phys.*, 2012, **14**, 3537.
30 P. F. Smet, A. B. Parmentier and D. Poelman, *J. Electrochem. Soc.*, 2011, **158**, R37.
31 G. Li, D. Geng, M. Shang, Y. Zhang, C. Peng, Z. Cheng and J. Lin, *J. Phys. Chem. C*, 2011, **115**, 21882.
32 W. Lv, Y. Jia, Q. Zhao, M. Jiao, B. Shao, W. Lü and H. You, *Advanced Optical Materials* 2014, ***2***, 183.
33 D. Kang, H. S. Yoo, S. H. Jung, H. Kim and D. Y. Jeon, *J. Phys. Chem. C*, 2011, **115**, 24334.